Electronic structure and lattice vibrations of $Ca_2CuO_2Cl_2$: A hybrid density functional study

C. H. Patterson
School of Physics, Trinity College Dublin, Dublin 2, Ireland
(Received 12 June 2007; revised manuscript received 24 December 2007; published 10 March 2008)

The electronic structure and phonon modes of $Ca_2CuO_2Cl_2$ have been calculated using hybrid density functional theory (HDFT) methods. The material is correctly predicted to be an antiferromagnetic insulator with a band gap of around 2 eV. Lattice parameters and atomic positions are in good agreement with experiment with a maximum error in lattice constant less than 2%. Phonon modes were calculated using HDFT Hamiltonians containing Hartree-Fock (HF) exchange with weights of 0.2, 0.3, or 0.4. Phonon mode frequencies typically shift upward by 4% on increasing the HF exchange weight by 0.1. Computed Cu-O stretching modes of E_u symmetry at 615 and 334 cm^{-1} are in good agreement with recently reported IR absorption frequencies at 620 and 350 cm^{-1}.

DOI: 10.1103/PhysRevB.77.115111 PACS number(s): 71.20.−b, 74.25.Jb, 74.25.Kc, 74.72.−h

I. INTRODUCTION

The oxychloride cuprate, $Ca_2CuO_2Cl_2$, is the parent compound for the series $Ca_{2-x}Na_xCuO_2Cl_2$, which is superconducting with optimal doping at $x=0.15$ and a T_c of 26 K.[1] Recently, it has been studied extensively using photoemission[2,3] and scanning tunneling microscopy (STM).[1,4] It has been selected for study because of the simplicity of its structure (it adopts the K_2NiF_4 structure, as does La_2CuO_4), it cleaves easily to give an atomically smooth, insulating CaCl surface layer, and it does not undergo a low temperature symmetry breaking distortion when doped with Na. All of these features make it ideally suited for photoemission and STM studies. When lightly hole doped with Na, $Ca_2CuO_2Cl_2$ exhibits stripes which are parallel to the Cu-O bond directions.[1]

Hybrid density functionals, which contain Hartree-Fock (HF) exchange with a weighting factor, have been tested in a range of insulating metal oxides.[5–15] In contrast to the local spin density approximation (LSDA) applied to cuprates,[16] hybrid functionals correctly predict parent compounds of doped cuprates to be antiferromagnetic insulators.[8–11] The B3LYP hybrid functional[17,18] predicts the band gap of a range of oxides quite accurately.[5,12] The weight of HF exchange in the B3LYP functional is 20%. In contrast, predictions for magnetic coupling constants in a range of oxides[7,8,11,13] show that the best agreement with experiment is obtained for a HF exchange weight of around 35%. Magnitudes of exchange constants predicted for cuprates using hybrid density functionals depend strongly on the weight of HF exchange used; in a range of insulating cuprates, predicted magnitudes of exchange coupling constants increased by a factor of around 20 on reducing the weight of HF exchange from 100% (unrestricted HF theory) to 0% (LSDA).[11]

The exchange-correlation energy in Becke's three parameter B3LYP hybrid functional[17,18] can be expressed as

$$E_{xc} = (1-A)(E_x^{LDA} + BE_x^{Becke}) + AE_x^{HF} + (1-C)E_c^{VWN} + CE_c^{LYP}, \quad (1)$$

where E_x^{LDA} and E_x^{Becke} are local density approximation[19] and Becke[17] exchange terms, E_x^{HF} is HF exchange, and E_c^{VWN} are the Vosko-Wilks-Nusair[20] and Lee-Yang-Parr[21] correlation functionals, respectively. The B3LYP hybrid functional has parameters $A=0.2$, $B=0.9$, and $C=0.81$, i.e., it contains HF exchange with a weight of 0.2. The CRYSTAL program[22] allows the A, B, and C parameters in hybrid density functional theory (HDFT) calculations to be varied. In this work, A was chosen to be 0.2, 0.3, or 0.4, i.e., the HF exchange in the Hamiltonian had 20%, 30%, or 40% of its weight in a self-consistent UHF calculation, while the B and C parameters were fixed at their standard values. Keeping B fixed while varying A means that the amount of Becke's exchange E_x^{Becke} changes too.

In the next section, we report the calculations of the crystal structure, electronic band structure, magnetic coupling constants, and phonons of $Ca_2CuO_2Cl_2$ using hybrid density functional methods. In particular, we investigate how the crystal structure and vibrational frequencies depend on the weight of HF exchange used in the functional. The B3LYP functional[17,18] and similar functionals, where the weight of HF exchange ranged from 20% to 40%, were used. The crystal structure was calculated using a conjugate gradient method in the CRYSTAL code[22] and frozen phonon calculations were performed at the equilibrium structures. Phonon frequencies for $Ca_2CuO_2Cl_2$ obtained using hybrid functionals are compared to frequencies from experiment and other calculations in the following section. Conclusions are given in the final section and details of calculations are given in the Appendix.

II. RESULTS

The space group for the oxyhalide cuprates is $I4/mmm$, No. 139, point group D_{4h}^{17}. The primitive unit cell contains one CuO_2 unit and any electronic structure calculation performed within this space group will necessarily result in a paramagnetic metal or ferromagnetic solution since the electron in the Cu $3d_{x^2-y^2}$ orbital will form a half-filled pair of bands or a filled band of one spin orientation. A density functional calculation on $Ca_2CuO_2Cl_2$ and $Ca_2CuO_2Br_2$ (Ref. 23) resulted in a paramagnetic solution. If the calculation is performed in the conventional unit cell for the $I4/mmm$ space group, $P4/mmm$, No. 123, point group D_{4h}^1, then an

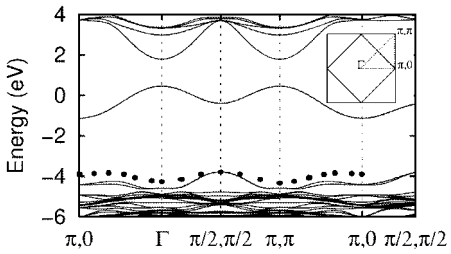

FIG. 1. Band structure for $Ca_2CuO_2Cl_2$. The inset shows the path in k space used for the band structure plot. The large square is the Brillouin zone for the 1×1 cell and the diamond is the Brillouin zone for the $\sqrt{2}\times\sqrt{2}$ supercell. The solid dots show the dispersion of the hole band in the t-J model redrawn from Ref. 24 using $J/t=0.4$ and $t=0.5$ eV.

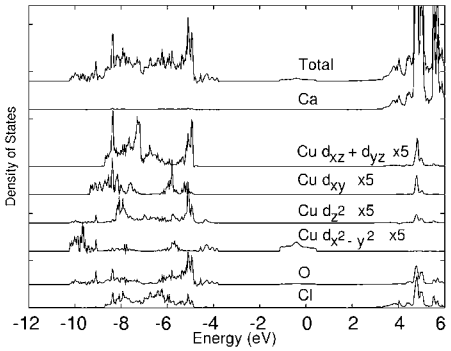

FIG. 2. The total density of states and atom or Cu d orbital-projected densities of states for $Ca_2CuO_2Cl_2$. Cu d orbital densities of states are scaled five times relative to others.

A-type antiferromagnetic solution can be obtained where CuO_2 planes are ferromagnetic but are stacked antiferromagnetically. This is referred to as an F unit cell in what follows because of the ferromagnetic coupling within CuO_2 planes. In order to obtain a solution that is antiferromagnetic within CuO_2 planes and insulating, a unit cell of at least $\sqrt{2}\times\sqrt{2}$ times the 1×1, tetragonal $P4/mmm$ unit cell must be adopted. The electronic band structure was calculated in this cell and phonon modes were calculated in the 1×1, $P4/mmm$ conventional cell, as well as in a 2×2 supercell. The latter frozen phonon calculations allow modes at the (π,π) and $(\pi,0)$ points of the 1×1 cell Brillouin zone to be calculated, as well as Γ point phonons. This is referred to as an A unit cell in what follows.

A. Electronic structure

The band structure for $Ca_2CuO_2Cl_2$, calculated using a $\sqrt{2}\times\sqrt{2}$ supercell, with the Cu magnetic moments arranged in an antiferromagnetic Néel state, is shown in Fig. 1. Dispersion of the hole band predicted by the t-J model for a CuO_2 layer with $J=0.4t$, redrawn from Ref. 24, is also shown in Fig. 1. A value of $t=0.5$ eV has been adopted, resulting in a t-J bandwidth of 0.55 eV. Overall, the shapes of the hole band dispersion predicted by the t-J model and by the HDFT calculation are in agreement. However, the bandwidth of 0.8 eV for the occupied $d_{x^2-y^2}$ band is greater than that measured by photoemission, 0.4 eV,[25] and predictions by the t-J model Hamiltonian at low hole concentration, 0.5 eV.[24] Energy eigenvalues in Fig. 1 have not been shifted to align the top of the valence band with any energy. The minimum single-particle band gap for $A=0.2(0.3)$, 2.6 eV (4.2 eV), is the indirect gap at $(\pi/2,\pi/2)/(\pi,0)$ and the minimum direct band gap for the same Hamiltonian parameters is 3.2 eV (4.9 eV) at $(\pi,0)$. The atom-projected density of states (Fig. 2) shows that the highest occupied band is predominantly of O $2p$ and Cu $3d_{x^2-y^2}$ character. Inspection of wave function coefficients shows that the band around −4 eV has mixed $d_{x^2-y^2}$ and O $2p$ character, except around the Γ point where it has O $2p$ character. Close inspection of the band structure shows an avoided crossing of states close to the Γ point for this band and O $2p$ bands just below. The vacant band around −1 eV is predominantly of Cu $3d_{x^2-y^2}$ character.

Energy differences between the ferromagnetic and antiferromagnetic states were evaluated at the equilibrium crystal structures of the antiferromagnetic states (see next section) with $A=0.2$ and $A=0.3$. In either case, an insulating state was predicted. The antiferromagnetic state was 160(143) meV lower in energy than the ferromagnetic state per f.u., when $A=0.2(0.3)$. These energy differences can be used to obtain an Ising Hamiltonian exchange constant, and in the case of a spin-half antiferromagnet on a square lattice, the exchange constant J is simply the energy difference of the antiferromagnetic and ferromagnetic states.[11] Ising magnetic coupling constants for $Ca_2CuO_2Cl_2$ obtained in this way are given in Table I and are taken from this work and earlier work by Munoz *et al.*[11] The magnetic coupling depends strongly on the weight of HF exchange used and the value obtained using LSDA is over 20 times greater than the UHF value and over five times larger than the typical experimental value for J in cuprates. Direct comparison of results for magnetic coupling constants between this work and the earlier work can only be made for the B3LYP calculations.

TABLE I. Dependence of magnetic coupling constant in $Ca_2CuO_2Cl_2$ on HF exchange weight in meV.

UHF[a,b]	35%[c]	30%[d]	B3LYP[d]	B3LYP[b]	LSDA[b]
32.5	127.7	143	160	190.6	702.3

[a]Experimental values of J for cuprates are typically 130 meV (Ref. 26).
[b]Reference 11.
[c]Weights used are 35% HF exchange 65% LDA exchange 100% LDA correlation (Ref. 11).
[d]This work.

TABLE II. $Ca_2CuO_2Cl_2$ bond lengths in Å. The weight of HF exchange in the Hamiltonian [i.e., the value of A in percent in Eq. (1)] and 1×1 ferromagnetic (F) or 2×2 antiferromagnetic (A) unit cells used are indicated at tops of columns.

Bond	Expt.	20 A	30 A	40 F
Cu-O	1.9344	1.9714	1.9675	1.9686
Cu-Cl	2.7539	2.7905	2.7770	2.7595
Ca-O	2.4902	2.5242	2.5163	2.5110
Ca-Cl		3.0409	3.0355	3.0319
Lattice const.	Expt.	20 A	30 A	40 F
a	3.8688	3.9429	3.9351	3.9372
c	15.0501	15.1245	15.05961	14.9646
Internal coord.	Expt.	20 A	30 A	40 F
Ca z	0.3958	0.3958	0.3958	0.3958
Cl z	0.1830	0.1845	0.1845	0.1844

Munoz *et al.* obtain a value of 190.6 meV which is somewhat larger than the value of 160 meV that we obtain. Both calculations used the CRYSTAL program[22] although the basis set used in this work had three sets of d functions per copper ion, whereas the earlier work had two sets.[11]

B. Crystal structure

The crystal structure of $Ca_2CuO_2Cl_2$ was calculated by energy minimization using the B3LYP functional, simultaneously varying atomic internal coordinates, and lattice parameters. Equilibrium lattice constants, internal coordinates, and bond lengths obtained using the standard B3LYP functional, as well as variations on this functional where larger weights of the HF exchange term than that in the B3LYP functional, are compared to experiment[27] in Table II.

When the standard B3LYP functional with 20% HF exchange is used, the a lattice constant is overestimated by 2%; increasing the weight of HF exchange in the functional to 40% results in a small reduction in this lattice constant. The c lattice constant is slightly overestimated by the standard B3LYP functional ($<1\%$) and the error in the c lattice constant remains below 1% when the weight of HF exchange is increased to 40%. All internal coordinates of ions except the Ca and Cl z coordinates are determined by symmetry. Values of these internal coordinates are in excellent agreement with experiment. The Cu-O bond length is overestimated by $<2\%$ and the Cu-Cl bond length is overestimated by up to 1.5%.

C. Phonon frequencies and eigenvectors

Phonon frequencies were calculated using a frozen phonon method in the CRYSTAL code[28] using the same hybrid density functionals, lattice parameters, and supercells used for crystal structure calculations. The macroscopic electric field is omitted from these calculations and so computed frequencies may best be compared with transverse optic modes. Modes with a $\mathbf{q}$ wave vector at the Γ point of the $I4/mmm$ Brillouin zone, calculated using 1×1 and 2×2 supercells, with various weights of HF exchange in the Hamiltonian are given in Table III. As noted above, calculations performed in a 1×1 cell, denoted F, have an A-type antiferromagnetism, while the 2×2 cell, denoted A, is antiferromagnetic within CuO_2 planes. There are seven ions in the primitive $I4/mmm$ unit cell and 18 phonon modes at the Γ point. E_u and A_{2u} modes are infrared (IR) active and A_{1g} and E_g modes are Raman active.

There is generally very good agreement between Cu-Cl mode frequencies calculated using either the 1×1 (F) or 2×2 (A) supercells with the same weight of HF exchange. Increasing the weight of the HF exchange in the hybrid func-

TABLE III. Γ point phonon frequencies for $Ca_2CuO_2Cl_2$ in cm^{-1}. The weight of HF exchange in the Hamiltonian [i.e., the value of A in percent in Eq. (1)] and 1×1 ferromagnetic (F) or 2×2 antiferromagnetic (A) unit cells used are indicated at tops of columns.

Symm.	Character	20 A	30 A	30 F	40 F
A_{1g}	Cu-Cl str.	320	326	326	331
	Cu-Cl str.	180	184	184	188
A_{2u}	Cu-O in phase buckling	392	407	398	414
	Cu-O in phase buckling	171	179	174	184
	Cu-Cl str.+Ca motion	153	157	157	162
B_u	Cu-O out of phase buckling	227	235	211	225
E_u	Cu-O str.	599	615	597	619
	Cu-O in plane bend	318	334	302	326
	CuO_4Cl_2+Ca motion	202	210	210	216
	Cu-Cl bend	111	115	115	118
E_g	Cu-Cl bend	182	187	188	191
	Cu-Cl bend+Ca motion	128	133	135	139

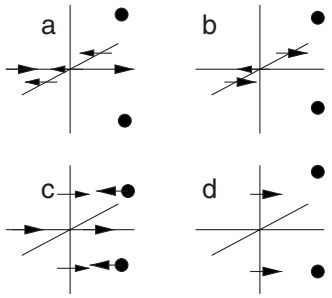

FIG. 3. Phonon eigenvectors for E_u modes at the Γ point. (a) Cu-O stretching, (b) Cu-O in plane bending, (c) CuO_4Cl_2+Ca motion, and (d) Cu-Cl bending.

tional shifts phonon mode frequencies upward typically by 4% for a 10% increase in HF exchange. However, there are significant differences between Cu-O mode frequencies using either supercell. This likely reflects the fact that Cu ions in CuO_2 planes are ferromagneticially coupled in the 1×1 cell, while they are antiferromagnetically coupled in the 2×2 supercell. The biggest difference between frequencies calculated using either 1×1 or 2×2 unit cells occurs for the B_u out of phase CuO_2 plane buckling mode and the E_u in plane Cu-O bending mode, where the 2×2 cell frequencies are roughly 10% higher than the 1×1 cell frequencies, indicating stronger Cu-O bonding in the A cell.

A recent IR study of $Ca_2CuO_2Cl_2$ (Ref. 29) found strong absorptions around 620 and 350 cm^{-1}. These likely correspond to the E_u modes we find at 615 and 334 cm^{-1} using the 2×2 cell with 30% HF exchange. Phonon eigenvectors for the E_u modes are shown schematically in Fig. 3. The 2×2 A unit cell contains phonon modes from the (0,0), $(\pi,0)$, $(0,\pi)$, and (π,π) points of the 1×1 Brillouin zone. Frequencies of Cu-O stretching and bending modes at these high symmetry points are given in Table IV. The E_u stretching mode at the Γ point at 615 cm^{-1} disperses downward slightly to 605 cm^{-1} at $(\pi,0)$. The other mode at $(\pi,0)$ and 640 cm^{-1} is a "half-breathing" mode where Cu-O stretching occurs along one Cu-O bond direction only. Modes where the vibrational motion is parallel to the wave vector have been labeled L for longitudinal in Table IV. The full breathing mode, where Cu-O stretching motions are in phase about each copper ion, is the highest frequency mode and occurs at 694 cm^{-1}. The E_u Cu-O in-plane bending mode at the Γ point disperses downward to 315 cm^{-1} at $(\pi,0)$ where it consists of a twisting motion of Cu-O bonds. The (π,π) in plane Cu-O bending motion at 478 cm^{-1} is a scissors motion of the CuO_4 unit in CuO_2 planes. The A_{2u} in phase buckling mode, in which oxygen ions move out of CuO_2 planes in phase, occurs at 407 cm^{-1} at the Γ point of the three-dimensional Brillouin zone. It disperses upward strongly to 495 cm^{-1} at $(0,0,\pi)$ where oxygen ions move in phase in the same CuO_2 plane, but motions of oxygen ions in neighboring planes are out of phase.

Finally, we comment on a mode which occurs at the (π,π) point of the Brillouin zone when the 2×2 supercell is used. Its eigenvector is shown schematically in Fig. 4 and it corresponds to rotations of O ions about Cu ions which change sense in a chessboard pattern. This mode occurs at 76 cm^{-1} when a Hamiltonian with 30% HF exchange is used, but when the weight of HF exchange is reduced to 20% it becomes unstable, i.e., it has an imaginary frequency and would lead to creation of a $\sqrt{2}\times\sqrt{2}R45°$ superlattice. Lattice distortions occur frequently in cuprates and have been associated with soft modes, although, as mentioned above, $Ca_2CuO_2Cl_2$ does not undergo this type of distortion, even when doped. The lattice instability for $Ca_2CuO_2Cl_2$ shown in Fig. 4 is different from that found in a phonon calculation for La_2CuO_4.[30] In that case the unstable mode at the X (π,π)

TABLE IV. Cu-O stretching and bending phonon frequencies above 250 cm^{-1} in $Ca_2CuO_2Cl_2$, calculated using a Hamiltonian with 30% HF exchange in an antiferromagnetic 2×2 unit cell. Modes marked L are longitudinal.

k point	Frequency (cm^{-1})
Stretching	
0,0	615
$\pi,0$	605
	640 (L)
π,π	694
	472
In-plane bending	
0,0	334
$\pi,0$	423 (L)
	315
π,π	478
Out-of-plane bending	
0,0	495
	407
$\pi,0$	328
	303
π,π	271

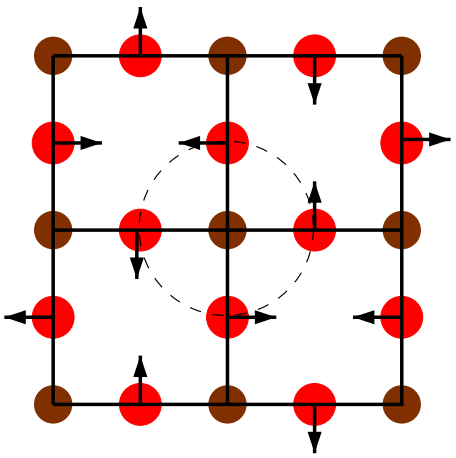

FIG. 4. (Color online) Phonon eigenvector for (π,π) Cu-O bending mode in the CuO_2 plane.

TABLE V. Comparison of Γ point phonon frequencies in cm^{-1} for $Ca_2CuO_2Cl_2$ (CCOC), $Sr_2CuO_2Cl_2$ (SCOC), and La_2CuO_4 (LCO) obtained from experiment and computation.

Symm.	CCOC[a]	SCOC[b]	LCO[b]	LCO[c]	LCO[d]	LCO[e]
A_{1g}	326			435	431	375
	184			228	208	202
A_{2u}	407			516	491	441
	179			354	361	182
	157			234	226	132
B_u	235				261	193
E_u	615	525	695	669	660	630
	334	351	400	359	360	319
	210	176	360		159	147
	115	140	145	148	120	22
E_g	187				256	201
	133				97	26

[a]This work, 30% HF exchange, and A unit cell.
[b]Reference 33. Data are from fits to optical reflectivity.
[c]Reference 30. Data are from fits to optical reflectivity.
[d]Reference 30. Data are from shell model calculation.
[e]Reference 34. Data are from first principles local density approximation calculation.

point of the Brillouin zone leads to a rigid tilting of the CuO_6 octahedra out of the CuO_2 plane. Neutron scattering[31,32] indicates that this instability is a consequence of a soft mode.

III. DISCUSSION

In this section, we compare computed frequencies for $Ca_2CuO_2Cl_2$ with frequencies for other cuprates with a similar structure, obtained from experiment and computation.

Phonon frequencies at the Γ point of the Brillouin zone from theory and experiment for three cuprates with similar structures are collected in Table V. $Ca_2CuO_2Cl_2$ A_{1g} mode frequencies are significantly below those of La_2CuO_4, as expected, since these are stretching modes involving apical ions of CuO_2Cl_2 or CuO_6 octahedra. There is considerable scatter in the predicted and measured frequencies for the A_{2u} modes. Predicted B_u out of phase CuO_2 plane buckling mode frequencies lie in a fairly narrow range, from 261 to 193 cm^{-1}. The E_u Cu-O stretching mode in La_2CuO_4 lies well above that in $Ca_2CuO_2Cl_2$ and it is perhaps surprising that substitution of Sr for Ca or Br for Cl makes such a large difference in Cu-O stretching frequencies. The shifts are −95 cm^{-1} on replacing Ca by Sr in $Ca_2CuO_2Cl_2$,[29,33] and −38 cm^{-1} on replacing Cl by Br in $Sr_2CuO_2Cl_2$.[33] E_g modes are Cu-apical ion bending modes and so E_g frequencies for $Ca_2CuO_2Cl_2$ are expected to lie below those of La_2CuO_4.

In Sec. II, we noted that increasing the weight of HF exchange in the calculation by 10% increases mode frequencies by around 4% for all stable modes. We also noted that an instability in the $Ca_2CuO_2Cl_2$ lattice, when a Hamiltonian with 20% HF exchange was used, was removed when the weight of HF exchange was increased to 30%. There are large differences in lowest energy E_u and E_g mode frequencies in La_2CuO_4 predicted by a local density calculation[34] (Table V, rightmost column) by a shell model calculation[30] (Table V) or observed in experiment.[32,33] In contrast to an unstable B_{2g} symmetry mode at the X point of the Brillouin zone, which is associated with a soft phonon at low temperature and whose softening has been attributed to anharmonicity in La_2CuO_4 force constants,[34] the E symmetry modes observed in experiment are stable at all temperatures. These large differences in E symmetry mode frequencies may be explained by overestimation of the electron gas polarizability in the local density calculation, leading to underestimation of mode frequencies, or even mode instabilities.

IV. CONCLUSIONS

The electronic structure, crystal structure, and phonon modes of $Ca_2CuO_2Cl_2$ were calculated using several hybrid density functional Hamiltonians with weights of HF exchange ranging from 20% to 40%. The former is the B3LYP functional. Phonon frequencies typically shift upward by 4% when the weight of HF exchange is increased by 10%. Frequencies of E_u symmetry Cu-O stretching and bending modes, calculated using a functional with 30% HF exchange, were 615 and 334 cm^{-1}, respectively. These frequencies are in good agreement with modes observed by IR spectroscopy at 620 and 350 cm^{-1}.[29] Phonon frequencies were calculated using 1×1 and 2×2 unit cells in which the Cu ions in CuO_2 planes were ferromagnetically (F) or antiferromagnetically (A) coupled. When calculations with the same HDFT Hamiltonian were repeated in either cell, Cu-Cl modes had nearly identical frequencies but some Cu-O modes shifted down-

ward in frequency by up to 10% in the F unit cell, indicating the importance of magnetic coupling in determining these mode frequencies.

ACKNOWLEDGMENTS

This work was supported by the Irish Higher Education Authority (IHEA) under the PRTLI-IITAC2 program. Computer time was provided by the Trinity Centre for High Performance Computing, which is supported by the IHEA and the Irish National Development Plan.

APPENDIX: DETAILS OF CALCULATIONS

HDFT calculations were performed using the CRYSTAL program.[22] Gaussian orbital basis sets used were standard all electron basis sets for Na,[35] Ca,[36] Cu,[37] O,[38] and Cl.[39] The Cu basis was supplemented by an extra *d* orbital with an exponent of 0.20 bohr^{-2} and the outer exponent of the standard Cu basis[37] was adjusted to 0.43 bohr^{-2}. The outer *sp* exponents of the Cl basis were modified to 0.294 and 0.090 bohr^{-2}. Tolerances for lattice sum convergence within the CRYSTAL program were chosen to be 7 7 7 7 14.

[1] T. Hanaguri, C. Lupien, Y. Kohsaka, D.-H. Lee, M. Azuma, M. Takano, H. Takagi, and J. C. Davis, Nature (London) **430**, 1001 (2004).
[2] F. Ronning, C. Kim, D. L. Feng, D. S. Marshall, A. G. Loeser, L. L. Miller, J. N. Eckstein, I. Bozovic, and Z.-X. Shen, Science **282**, 2067 (1998).
[3] F. Ronning *et al.*, Phys. Rev. B **67**, 165101 (2003).
[4] Y. Kohsaka *et al.*, Science **315**, 1380 (2007).
[5] F. Cora, M. Alfredsson, G. Mallia, D. Middlemiss, W. C. Mackrodt, R. Dovesi, and R. Orlando, Struct. Bonding (Berlin) **113**, 171 (2004).
[6] I. D. R. Moreira and R. Dovesi, Int. J. Quantum Chem. **99**, 805 (2004).
[7] X.-B. Feng and N. M. Harrison, Phys. Rev. B **70**, 092402 (2004).
[8] R. L. Martin and F. Illas, Phys. Rev. Lett. **79**, 1539 (1997).
[9] X.-B. Feng and N. M. Harrison, Phys. Rev. B **69**, 132502 (2004).
[10] J. K. Perry, J. Tahir-Kheli, and W. A. Goddard, Phys. Rev. B **63**, 144510 (2001).
[11] D. Munoz, I. de P. R. Moreira, and F. Illas, Phys. Rev. B **65**, 224521 (2002).
[12] C. H. Patterson, Phys. Rev. B **74**, 144432 (2006).
[13] I. P. R. Moreira, F. Illas, and R. L. Martin, Phys. Rev. B **65**, 155102 (2002).
[14] R. Dovesi, R. Orlando, C. R. C. Pisani, and V. R. Saunders, Phys. Status Solidi B **217**, 63 (2000).
[15] F. Cora, Mol. Phys. **103**, 2483 (2005).
[16] D. J. Singh and W. E. Pickett, Phys. Rev. B **44**, 7715 (1991).
[17] A. D. Becke, J. Chem. Phys. **98**, 5648 (1993).
[18] P. J. Stephens, F. J. Devlin, C. F. Chabalowski, and M. J. Frisch, J. Phys. Chem. **98**, 11623 (1994).
[19] P. A. M. Dirac, Proc. Cambridge Philos. Soc. **26**, 376 (1930).
[20] S. H. Vosko, L. Wilk, and M. Nusair, Can. J. Phys. **58**, 1200 (1980).
[21] C. Lee, W. Yang, and R. G. Parr, Phys. Rev. B **37**, 785 (1988).
[22] R. Dovesi *et al.*, *Crystal06 User's Manual* (University of Torino, Torino, 2007) (www.crystal.unito.it).
[23] L. F. Mattheiss, Phys. Rev. B **42**, 354 (1990).
[24] E. Dagotto, A. Nazarenko, and M. Boninsegni, Phys. Rev. Lett. **73**, 728 (1994).
[25] K. M. Shen *et al.*, Phys. Rev. Lett. **93**, 267002 (2004).
[26] B. Keimer, N. Belk, R. J. Birgeneau, A. Cassanho, C. Y. Chen, M. Greven, M. A. Kastner, A. Aharony, Y. Endoh, R. W. Erwin, and G. Shirane, Phys. Rev. B **46**, 14034 (1992).
[27] D. N. Argyriou, J. D. Jorgensen, R. L. Hitterman, Z. Hiroi, N. Kobayashi, and M. Takano, Phys. Rev. B **51**, 8434 (1995).
[28] F. Pascale, C. Zicovich-Wilson, F. Lopez, B. Civalleri, R. Orlando, and R. Dovesi, J. Comput. Chem. **25**, 888 (2004).
[29] T. Hasegawa, N. Ogita, T. Kondo, Y. Zenitani, H. Kawashima, T. Suzuki, J. Akimitsua, and M. Udagawa, Low Temp. Phys. **32**, 533 (2007).
[30] M. Mostoller, J. Zhang, A. M. Rao, and P. C. Eklund, Phys. Rev. B **41**, 6488 (1990).
[31] R. J. Birgeneau *et al.*, Phys. Rev. Lett. **59**, 1329 (1987).
[32] P. Boni, J. D. Axe, G. Shirane, R. J. Birgeneau, D. R. Gabbe, H. P. Jenssen, M. A. Kastner, C. J. Peters, P. J. Picone, and T. R. Thurston, Phys. Rev. B **38**, 185 (1988).
[33] S. Tajima, T. Ido, S. Ishibashi, T. Itoh, H. Eisaki, Y. Mizuo, T. Arima, H. Takagi, and S. Uchida, Phys. Rev. B **43**, 10496 (1991).
[34] C.-Z. Wang, R. Yu, and H. Krakauer, Phys. Rev. B **59**, 9278 (1999).
[35] R. Dovesi, C. Roetti, C. Freyria-Fava, M. Prencipe, and V. Saunders, Chem. Phys. **156**, 11 (1991).
[36] W. C. Mackrodt, Philos. Mag. A **68**, 653 (1993).
[37] K. Doll and N. M. Harrison, Chem. Phys. Lett. **317**, 282 (2000).
[38] M. D. Towler, N. L. Allan, N. M. Harrison, V. R. Saunders, W. C. Mackrodt, and E. Aprà, Phys. Rev. B **50**, 5041 (1994).
[39] E. Apra, M. Causa, M. Prencipe, R. Dovesi, and V. Saunders, J. Phys.: Condens. Matter **5**, 2969 (1993).